ISIJ International, Vol. 50 (2010), No. 6, pp. 883–892

Analytical Investigation on Ultimate Behaviors for Steel Heavy Clip-angle Connections Using FE Analysis

Jong Wan HU,[1] Roberto T. LEON[2] and Taehyo PARK[1]

1) Department of Civil Engineering, Hanyang University, Seoul, 133-791, Korea. E-mail: cepark@hanyang.ac.kr
2) School of Civil and Environmental Engineering, Georgia Institute of Technology, Atlanta, GA, 30332-0355, USA.

(*Received on December 1, 2009; accepted on April 12, 2010*)

This paper describes an analytical investigation on the strength, stiffness, and mechanical behavior of heavy clip-angle connections subjected to static loading. The work is based on the results of a large experimental investigation into the cyclic behavior of connection components incorporating with thick clip-angles. The results of these tests are described first, and then methodologies to generate the response of connection components, utilizing nonlinear finite element (FE) models with the advanced modeling methods such as the pretension force in the bolts and the interaction between two contact surfaces, are presented in this study. Numerical test results obtained from FE analyses are compared with experimental test results in an effort to verify that 3D FE models can simulate the overall and detailed behavior of a various type of clip-angle connections accurately. These FE models provide useful instrumentation, which is difficult to obtain during an experiment, such as the distribution of the plastic strain, prying forces induced by the initial bolt pretension, and friction forces on the interface between a clip-angle and a steel beam. These valuable results can support the basic knowledge for developing strength models consistent with the AISC-LRFD component method of the clip-angle design. They are also utilized to better understand the parametric effect of connection components and achieve a comprehensive study of their behavior.

KEY WORDS: finite element (FE) analysis; heavy clip-angle connection; tension bolts; bolt pretension; prying force.

1. Introduction

Two major earthquakes in 1994 and 1995, the Northridge and Kobe earthquakes, highlighted the vulnerability of conventional welded connections in steel moment frames and drew attention to the role that partial strength (PS), partially restraint (PR) connections played in the post-fracture behavior of those structures.[1] As a result, several research projects have been carried out to supplement the drawbacks in welded beam-to-column connection designs and to investigate alternative PR bolted connections.[2–8] T-stub or endplate connections have been widely used in modern moment frames as alternatives to fully welded connections for medium to heavy weight beam sizes.[6–8] For clip-angle connections, stronger and stiffer clip-angles should be required at the connection design so as to use them in low to mid-rise modern structures. However, most existing researches for clip-angle connections have been focused on the connection designs that utilize light to medium angles (t_f=6 to 16 mm) for fastening the steel beams to the column by high strength bolts.[9–14]

SAC Subtask 7.03[15,16] was conducted at the Georgia Institute of Technology and focused on steel bolted clip-angle connections in order to introduce heavy clip-angles (t_f=25 mm) to the connection design. The cyclic behavior of clip-angle connections was studied both at component and full-scale connection tests. A discussion of the experimental programs was provided by Swanson[15] and Schrauben.[16] However, the data obtained from a series of component tests was not applied to the design recommendation and no analytical study for those test models was performed in those studies.

The research reported herein follows previous one presented by Swanson *et al.*,[17] Hu and Leon,[18] and Hu[19] who used three dimensional (3D) FE models both to investigate the prying response of tension bolts and to predict the deformation of T-stub and top-and-seat angle connections under static axial loading. Citipitioglu *et al.*[20] studied the effect of slip by using a general contact scheme in similar connection models and presented extensive-parametric 3D FE analysis of PR bolted connections.

FE analyses, which are supplemented by the experimental data, are intended to provide a better understanding of the component behavior. In this study, the refined 3D modeling of heavy clip-angle components were performed to recognize the basic mechanism of heavy clip-angle behavior and the stress distribution by means of the results obtained from FE analyses. The experimental test results provided by the SAC Subtask 7.03 project[15,16,18] were investigated and compared with the numerical test results. This paper concentrates on examining the basic mechanism for heavy clip-angle connections including the prying action due to the bolt pretension. The ultimate strength capacities of heavy clip-angle components obtained from static FE

analyses are also investigated to evaluate currently accepted strength models for bolted connection designs.

2. Prying Model

The prediction of the ultimate strength for PR connections is a quite complex process because several yielding or failure modes interact with one another and are tied to uncertainties in both material properties and fabrication tolerances. Among the possible failure modes, the most studied cases are related to the bending action in the clip-angle leg associated with the bolt pretension. This prying mechanism can be followed by the ultimate failure of tension bolts (*i.e.* bolt fracture) or the yield failure of components (*i.e.* flange yielding). In this study, the prying action in the clip-angle leg will be addressed and the existing prying model used in the AISC-LRFD[21] will be estimated by comparing its strength predictions with FE analysis results that were calibrated to the experimental test results of steel clip-angle components. This prying model was based upon one of the most widely used models developed by Kulak *et al.*[22]

As shown in **Fig. 1**(a), prying action refers to the additional forces due to the reactions at the tip of the uplifting angle leg (Q); these additional forces can increase the tension in the bolts ($\sum B_n$) and lead to premature failure. They effectively reduce the load applied to the clip-angle (P). The static equilibrium exists in this mechanism ($\sum B_n = P+Q$). In general, the prying force (Q) acting on the tip of the angle leg can be minimized by either increasing the member thickness (t_f) or reducing the tension bolt gauge length (g_t). Figure 1(b) shows the notation and dimensions used in the prying model for the determination of the ultimate strength of the clip-angle. In this model, the bolt forces are assumed to act at the inside edge of the bolt shank instead of acting at the centerline of the bolt shank. This premise is based on the assumption that more of bolt head pressure is distributed into the angle leg under the inside of the bolt head than under the outside of the bolt head.[21,22] As a result, static equilibrium should be based on the parameters a' and b' instead of a and b. The magnitude of a is limited to a value no greater than $1.25b$ in this model.[22]

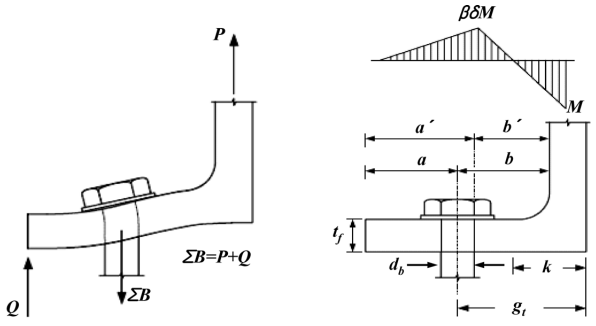

Fig. 1. Typical flange prying action for component members.

Based upon considering three possible failure modes shown in **Fig. 2**, the ultimate capacity of the component members is computed. These three failure modes can be expressed by Eqs. (1) to (3). They correspond to formation of a plastic mechanism on the flange (Eq. (1)), bolt prying mixed with flange yielding (Eq. (2)),[23] and tension bolt fracture without the prying force (Eq. (3)), respectively:

$$P = \frac{(1+\delta)W_{\text{Clip}}F_y t_f^2}{4b'} \quad \text{.....(1)}$$

$$P = \frac{\sum B_{n,\text{tension}}a'}{a'+b'} + \frac{W_{\text{Clip}}F_y t_f^2}{4b'} \quad \text{.....(2)}$$

$$P = \sum B_{n,\text{tension}} \quad \text{.....(3)}$$

where t_f is the thickness of clip-angle legs; F_y is the yielding stress of carbon steel (for FE350, F_y=350 MPa); W_{Clip} is the width of the clip-angle (see Fig. 4); $B_{n,\text{tension}}$ is the tensile capacity of tension bolts (*cf.* the tensile strength of a bolt ($F_{n,\text{tension}}$): 780 MPa for M10.8 bolt and 620 MPa for M7.2 bolt).[21] δ is the ratio of the net section area to the gross section area, excluding the fillet, and can be written as:

$$\delta = 1 - \frac{2d_h}{W_{\text{Clip}}} \quad \text{.....(4)}$$

where d_h is the diameter of bolt holes.

The parameter for the level of the prying present (β, see Fig. 1(b)) is defined as the ratio of the moment on the bolt centerline to the moment on the face of the angle leg.[15,22] When this parameter exceeds unity ($\beta \geq 1$), the thickness of the flange is sufficient to cause the plastic flange mechanism to form as if the flange were a fixed–fixed beam (see Fig. 2(a)). When $\beta \leq 0$, the upstanding angle leg is separated from the contact surface (see Fig. 2(c)). The prying forces are zero and the bolts are subjected to only conventional tension without bending moment. The bolt fracture results

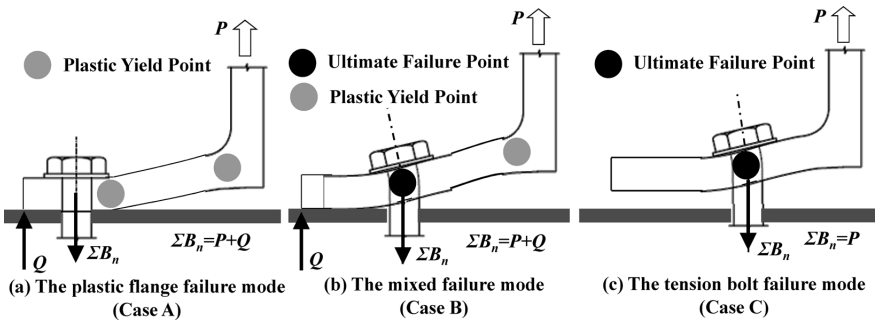

Fig. 2. Three possible failure modes under the tension force.

in the dominant failure mode. Finally, if $0 \le \beta \le 1$, then a combination of flange yielding and bolt prying will occur at the clip-angle leg (see Fig. 2(b)). The static and moment equilibrium on the clip-angle leg presented in Fig. 1 can be written as:

$$\sum B_n = P + Q \quad \text{.....(5)}$$

$$Pb' = (1+\beta\delta)M \quad \text{.....(6)}$$

$$Qa' = \beta\delta M \quad \text{.....(7)}$$

At the plastic mechanism, M_p results in the plastic capacity of the clip-angle leg and can be written as:

$$M_P = \left(\frac{W_{\text{Clip}} t_f^2}{4}\right) F_y \quad \text{.....(8)}$$

Substitution of the plastic moment, M_p, into Eq. (6) yields β, which is written as the function of the applied axial force, P, as shown in the below equation.

$$\beta = \left(\frac{1}{\delta}\right)\left(\frac{4Pb'}{W_{\text{Clip}} t_f^2 F_y} - 1\right) \quad \text{.....(9)}$$

The prying force (Q) can be derived by manipulating the equilibrium equation, Eq. (7), as follow:

$$Q = \left(\frac{Pb'}{a'}\right)\left(\frac{\beta\delta}{1+\beta\delta}\right) \quad \text{.....(10)}$$

The general solution for the determination of the clip-angle capacity can be plotted as a function of the angle thickness (t_f). **Figure 3** represents a theoretical solution space for flange yielding and bolt prying of a typical clip-angle. The line segment OC is defined by the plastic mechanism of the clip-angle leg and is computed using Eq. (1) with the assumption that $\beta = 1.0$. The line segment CD represents the bolt capacity including the effect of the bolt prying and is calculated using Eq. (2). The line segment DE represents the conventional bolt tension strength without any prying action and is calculated using Eq. (3). Therefore, when $0 \le \beta \le 1$, the bold line OCDE represents the capacity of the clip-angle and tension bolts and the region below this line represents the adequate design strength.[15,21,22]

The thickness of the clip-angle presented in this study ($t_f = 25$ mm) is associated with the line segment OB which represents a plastic failure mechanism of the clip-angle leg with a value of $\beta = 1.62$. Since this case is outside the physical range of 0 to 1, the expanded solution region should be used to determine the ultimate strength capacity.[15,21–23] The dash line ABC represents the bolt failure after a plastic mechanism on the clip-angle leg has been established. Therefore, the line segment OC, which indicates the plastic flange mechanism, results in the theoretical and preliminary failure mode but does not results in the ultimate failure based on the ultimate strength of tension bolts. After exceeding the limit of the plastic mechanism on the line segment OC, the strain hardening of the base clip-angle material provides additional strengths until tension bolts fail by ultimate fracture. As a result, the point B represents the ultimate capacity of the clip-angle component with a value of $t_f = 25$ mm (*i.e.* approximately $P = 390$ kN). This physical mechanism will be verified through the observation of the plastic strain distribution obtained from FE analysis results. It will be also shown that the ultimate capacity of heavy clip-angles investigated in this study mostly lies above the line segment ABC.

3. Experimental Overview

As part of the SAC Task 7.03 project, Swanson[15] tested 10 thick angle components. The typical dimensions of specimens by Swanson are given in **Fig. 4**. Details of the component tested are summarized in **Table 1**, along with the ultimate strength obtained in the experimental tests.

The behavior of thick clip-angles is controlled by the prying action of tension bolts. The prying capacity is primarily governed by the geometric ratio H_1 to H_2 (see Fig. 4), which determines the ultimate capacity, the bolt failure mode, and the extent of the bending mechanism in the clip-angle. Additional parameters (*i.e.* the width of the bolt head, the length of the bolt shank, the type of bolts used, and the alignment of shear bolts in its oversize hole) are often needed to model the behavior in detail. All specimens summarized in Table 1 ultimately failed by bolt fracture. Component tests were all run under cyclic loads. The en-

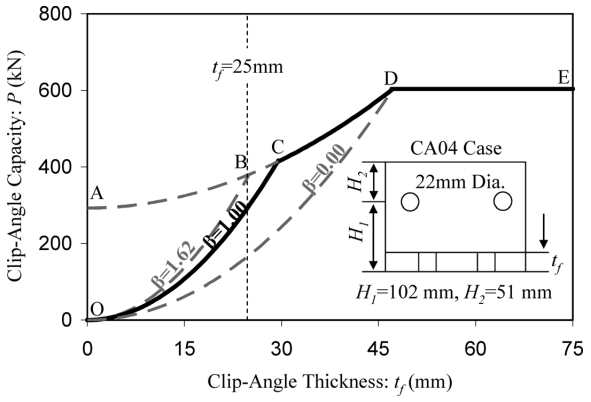

Fig. 3. General solution for clip-angle capacity based on failure modes.

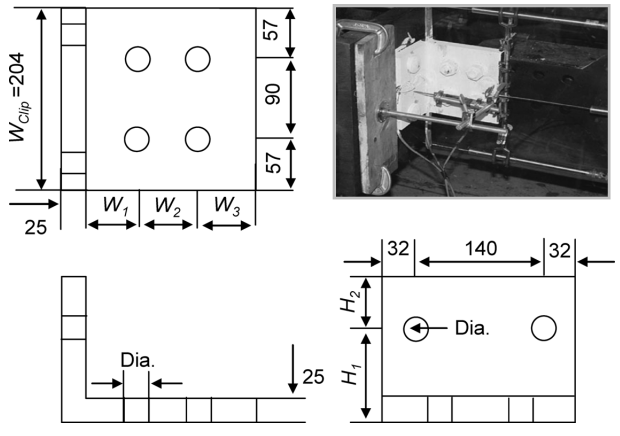

Fig. 4. Component details (mm).

Table 1. Geometric size of component specimens.[15)]

Model	W_1	W_2	W_3	H_1	H_2	Bolt (diameter x length)	Grade***	Ultimate Strength (Test, kN)
CA01	56	67	56	64	38	22 x 114 (T)*, 22 x 89 (S)**	M 10.8	482
CA02	56	67	56	64	89	22 x 114 (T), 22 x 89 (S)	M 10.8	557
CA04	56	67	56	102	51	22 x 114 (T), 22 x 89 (S)	M 10.8	375
CA09	51	76	51	64	38	25 x 102 (T), 25 x 114 (S)	M 10.8	557
CA10	51	76	51	64	89	25 x 114 (T), 25 x 114 (S)	M 10.8	709
CA12	51	76	51	102	51	25 x 114 (T), 25 x 114 (S)	M 10.8	486
CA14	51	76	51	64	89	25 x 114 (T), 25 x 114 (S)	M 7.2	609
CA16	51	76	51	102	51	25 x 114 (T), 25 x 114 (S)	M 7.2	424
CA17	56	67	56	64	89	22 x 108 (T), 25 x 89 (S)	M 10.8	538
CA18	56	67	56	64	89	22 x 102 (T), 25 x 89 (S)	M 10.8	530
BC's	Stiffened W360X382 Column stub, 152 x25 plate used for a beam flange							
Steel Grade	FE 350(Grade 50) Carbon Steel							
Beam Setback	Each 48mm (22mm Bolt Dia.) and 38mm (25mm Bolt Dia) Beam Setback.							
Diameter	Adding clearance (1.6mm) to the diameter of bolt							

* (T) = Tension bolts ** (S) = Shear bolts *** = Grade for used bolts M10.8 = ASTM A490; M7.2 = ASTM A325

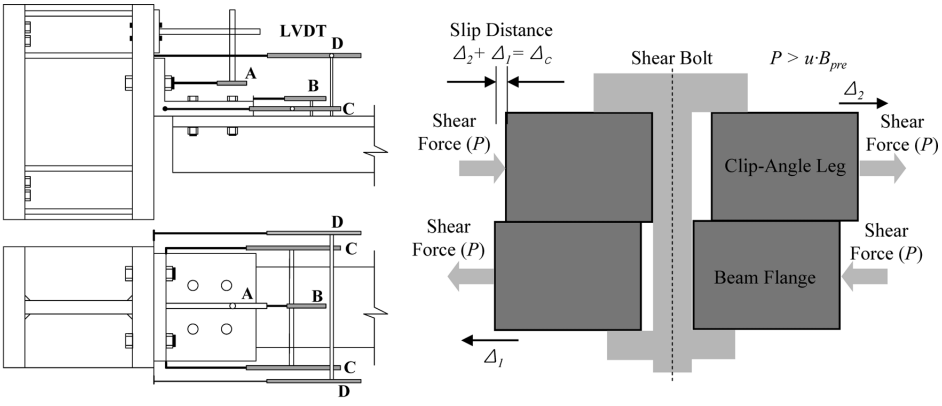

(a) Instrumentation Scheme for Experimental Tests (b) Measurement of the Slip Distance on the Shear Faying Surface

Fig. 5. Instrumentation scheme and slip measurement of clip-angle component tests.

velopes of cyclic response will be used for comparison with FE analysis results which were obtained from monotonic loading tests.

The component tests were extensively instrumented with displacement transducers (LVDTs). Each pair of LVDT shown in **Fig. 5**(a) monitored individual displacements which were used to isolate the different components of the overall deformation. LVDTs A monitored the uplift of the upper clip-angle from the face of a column, while LVDTs B measured the slip deformation between the clip-angle and the beam flange. Slip mechanism due to the direct shear force acting on the slip plane is illustrated in Fig. 5(b). Once this slip force exceeds the slip resistance provided by the clamping force, slip between two surfaces of bolted component starts to occur (*e.g.* $P > u \cdot P_{pre}$). As shown in Fig. 5(b), the clamping force is estimated by the product of the friction coefficient and the bolt pretension ($u \cdot B_{pre}$). Slippage occurs because construction tolerances (Δ_c) require that bolt holes should be at least 1.6 mm larger than the nominal bolt diameter (d_b). Once this tolerance is exceeded, the bolt begins to bear on the plates and the stiffness and strength increase again. LVDTs C measured the elongation of the clip-angle leg. Finally, LVDTs D measured the overall clip-angle deformation consisting of these three deformation mechanisms.

4. 3D FE Models

Three dimensional non-linear finite element analyses (3D FE) were carried out using ABAQUS[24)] in order to estimate the response of bolted PR connections such as those described in the tests above. The clip-angle components (CA01 to CA18) were modeled using C3D8 (eight node solid) elements. The inner core of bolts and the K-zone of clip-angles are modeled by C3D6 (6 node wedge element). Over 5500 elements and 22 650 degrees of freedoms (DOF) were typically used in modeling these components. These 3D FE connections had three bolts and 4 different kinds of components (*i.e.* Clip-angle, Beam, Column, and Nut). The 3D FE simulations consisted of over 26 500 elements and 355 000 DOFs. A typical mesh is shown in **Fig. 6**. The connections were modeled as half models with symmetric boundary conditions in order to save computation time and cost.

Component models applied typical material properties shown in **Fig. 7** to FE analyses.[15,16)] The material properties of test specimens such as M10.8 (A490) and FE350 (A572-Gr. 50) were fully nonlinear. The stress–stress curve for a

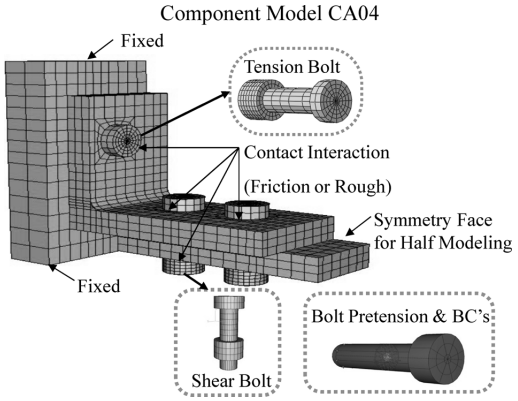

Fig. 6. FE models for clip-angle component (CA04 model).

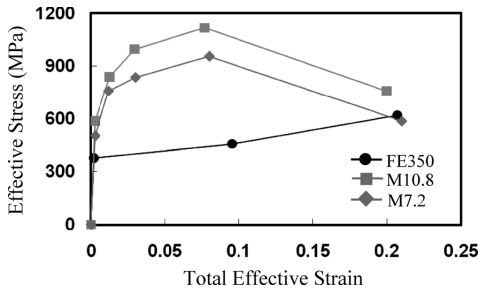

Fig. 7. Material properties for FE analyses.

M7.2 (A325) bolt was also made up of this research.

All models incorporated contact interaction with either a friction or rough condition between adjacent surfaces. Rough conditions, which do not permit slip deformation to occur, were specified at two locations: (1) between the underside of the bolt head and the clip-angle surrounding the tension bolt holes, and (2) between the shanks of the shear bolts and the contiguous inside portion of the nut hole. A rough condition at the nut hole led to an increase in slip resistance and caused the nut head which comes into contact with the beam flange. All other contact surfaces utilized friction conditions with the value of 0.25 for the friction coefficient.

The pretension in the bolts and friction was significant parameters in these bolted connections. Great care was taken to attempt to model the bolt behavior correctly, including the oversize holes (bolt clearance of 1.6 mm). To pretension the bolts, a prescribed bolt displacement was imposed with the value of 0.25 mm at the middle of the bolt shank while holding the bolt end fixed to a fictitious plane during the first loading step. The tip of the bolt, which was fully restrained during the first load step, was released during the second load step which was used to impose the monotonic loading at the tip of the beam. Friction on the contact surface between the bottom of the clip-angle and the upper of the beam flange was the main source of force transfer before the slip load was reached. Sliding between the beam flange and the clip- angle occurred after the applied loading exceeded the slip resistance. A number of these modeling methods were generated in order to improve the numerical stability for the computations under static loads, which are the ultimate goal of this research.

5. Comparisons between Experimental Results and Analytical Results

Ten graphs shown in **Fig. 8** represent selected comparisons for applied force *vs.* overall clip-angle deformation between the experimental test results and the FE analysis results. For similar geometries, the effect of the bolt size is clearly seen when comparing Figs. 8(a) and 8(d), Figs. 8(b) and 8(e), and Figs. 8(c) and 8(f). Each of these pairs was an identical component with the bolt diameters (d_b) of 22 mm and 25 mm, respectively. The larger bolts can lead to larger angle capacities, with increases approximately ranging from 15 to 30%.

The amount of this increase is tied to the prying force, as can be seen from comparing Figs. 8(b) and 8(c), and Figs. 8(e) and 8(f), with ratios of H_1/H_2 of 0.72 and 2.00, respectively. The smaller H_1/H_2 results in larger increases since the prying forces do not build up as quickly. Therefore, the larger prying forces cause to reduce the ultimate angle capacities. The difficulty in properly reproducing the slip behavior can be seen from comparing Figs. 8(b) and 8(c) (*i.e.* specimens CA-02 and CA-04). In the experimental results, CA-02 has a clear slip plateau at about 330 kN, while CA-04 shows a combination of slip and yielding around 380 kN; the analyses both clearly show these plateaus, but the magnitude is smaller in the case of CA-04. The predictions of both ultimate load and ultimate deformation given by the FE models appear to be excellent. Both compared results show good agreements in terms of initial slope, slip behavior, yield strength, and ultimate strength.

6. Observations of 3D FE Analyses

6.1. Deformation

Figure 9 shows the deformed configuration of the CA04 component, near their ultimate loading stage. The monotonic load was imposed by pulling on the beam component in tension along its centroid. Both compared clip-angle models (Experimental test model *vs.* FE model) show good agreement with respect to deformed shapes. CA04 specimen was designed with a relatively larger ratio of H_1/H_2. Therefore, the prying action is clear from the deformed shapes shown in the figures and led to tension failures of the bolts as had been observed in the experimental test results. Distinct bolt prying action can be verified by this deformed configuration due to bending effect observed near the bolt head (see a deformed tension bolt in Fig. 9(b)).

The figures also show the plastic stress contours, which indicate that a plastic stress hinge occurred in the vertical clip-angle leg adjacent to the toe of the fillet area and that the thickness of the angle resulted in the bolt head lifting and bending (see a dotted circle in Fig. 9(b)). A plastic hinge also occurred in the underneath of the bolt head because of bending effect. It indicates that this steel heavy clip-angle connection was designed with sufficient ductility. In addition, the area around the bolt hole has yielded.

6.2. Prying Action Mechanism

FE analyses are able to extend the study of clip-angle components with more details on the parametric effect beyond the experimental data. FE analysis results are exten-

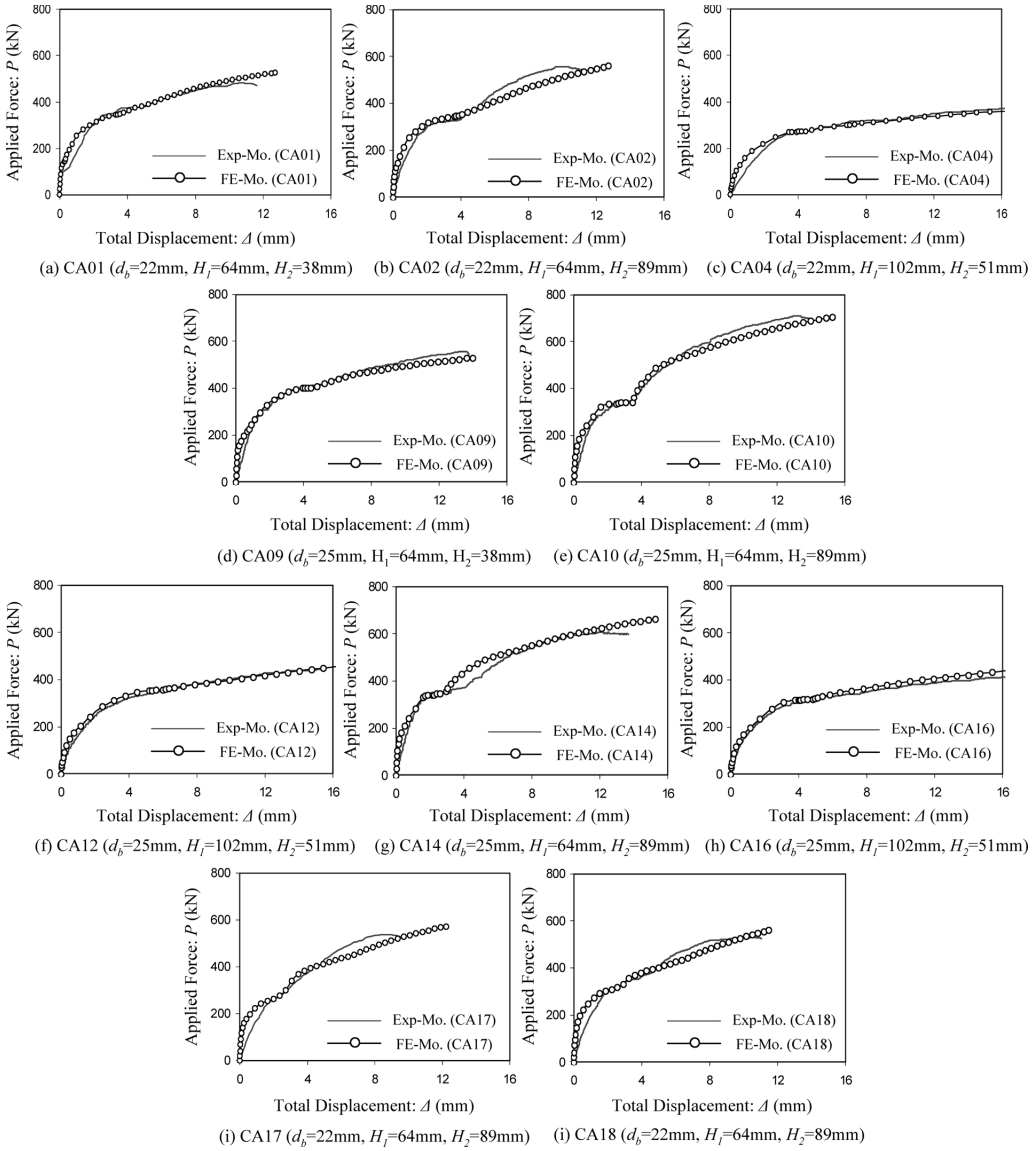

(a) CA01 (d_b=22mm, H_1=64mm, H_2=38mm) (b) CA02 (d_b=22mm, H_1=64mm, H_2=89mm) (c) CA04 (d_b=22mm, H_1=102mm, H_2=51mm)

(d) CA09 (d_b=25mm, H_1=64mm, H_2=38mm) (e) CA10 (d_b=25mm, H_1=64mm, H_2=89mm)

(f) CA12 (d_b=25mm, H_1=102mm, H_2=51mm) (g) CA14 (d_b=25mm, H_1=64mm, H_2=89mm) (h) CA16 (d_b=25mm, H_1=102mm, H_2=51mm)

(i) CA17 (d_b=22mm, H_1=64mm, H_2=89mm) (i) CA18 (d_b=22mm, H_1=64mm, H_2=89mm)

Fig. 8. Total displacements from experimental and FE models for clip-angle components.

sively used to study the effect of bolt pretensioning and prying action on the response of tension bolts, clip-angles, and even full-scale connections.

The response of tension bolts obtained from theoretical calculations and FE analysis results is shown in **Fig. 10**. The multi-linear line in the figure represents the tension bolt response under zero pretension and no prying action, while other two curves drawn by the measurement from FE models represent the reaction force-deformation response of one tension bolt with the initial pretension. The behavior of the tension bolts with negligible bending moments is highly dependent on the material properties and mimics the behavior of a tensile coupon. However, after the first yield transition point, two curves from FE analyses cannot reach this anticipated strength of a bolt only pulled. Specimens designed with the relatively larger bolt prying force (*i.e.* CA04 and CA12) have smaller bolt's tensile capacity than those designed with relatively smaller one (*i.e.* CA02 and CA10) as shown in Figs. 10(a) and 10(b). They start at non-zero forces because the bolts are initially pretensioned.

The more detail investigation into the prying response of tension bolts is shown in **Fig. 11**. The solid lines in the figure represent the response of the tension bolts with no prying and zero pretension. The prying forces according to the geometric ratio of H_1/H_2 are simply estimated by using this prying response of tension bolts compared. At the beginning of the loading step, the response of the tension bolts is dominantly affected by the initial pretension of tension bolts. As the total applied force increases, the reaction force in the bolts subjected to the tension also increases. Moreover, the amount of the prying force at the ultimate state is highly dependent on the geometric ratio of H_1/H_2 in the clip-angle. As mentioned in the static equilibrium, the prying force, which builds up quickly, causes to increase the tension reaction force in the bolts. Therefore, specimens with the larger H_1/H_2 such as CA04 and CA12 are more susceptible to the bolt fractures.

In order to investigate plastic hinge sequences and failure modes in the clip-angles, the plastic equivalent strain fields are compared under the ascending steps (G_1=200 kN, G_2=400 kN, G_3=500 kN, and final loading step) graphically illustrated in Fig. 11. These plastic strain fields (PEEQ) are shown in **Fig. 12**. As shown in the first loading step G_1, the plastic strain starts to occur at around bolt

holes and bolt shanks. The plastic strain fields spread to the fillet area and the clip-angle leg at the second loading step G_2. Approximately 3.5% maximum plastic strain contours, which indicate that a plastic hinge starts to occur, are found at the fillet area of the CA12 specimen after bearing deformation occurs at around 400 kN. In addition, the plastic strain field concentrates around the bolt hole. Therefore, it is clearly assured that CA12 specimen under this loading step undergoes the plastic flange mechanism, as the preliminary failure, corresponding to the failure mode, CASE A, illustrated in Fig. 2(a). At the final loading step, the bolt fracture mixed with the plastic hinge is commonly observed at all specimens shown. This failure state, as the ultimate failure mode, was graphically described in the mixed failure mode, CASE B, illustrated in Fig. 2(b). As compared with other specimens, CA12 specimen has the most extensive area of the plastic strain field among three compared specimens under the same level of the loading step.

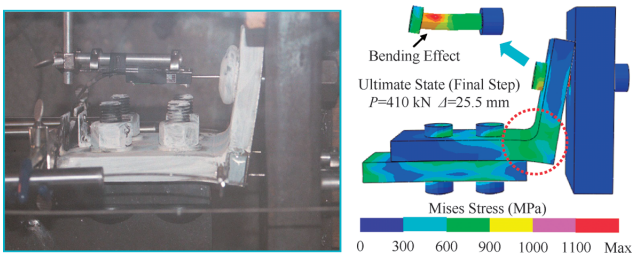

(a) Experimental Test Result (b) FE Analysis Result

Fig. 9. Comparison of a deformation configuration.

7. Performance Based Evaluations for Heavy Clip-angles

Several limit states based on the failure modes have been used for a clip-angle design. Some are ultimate limit states

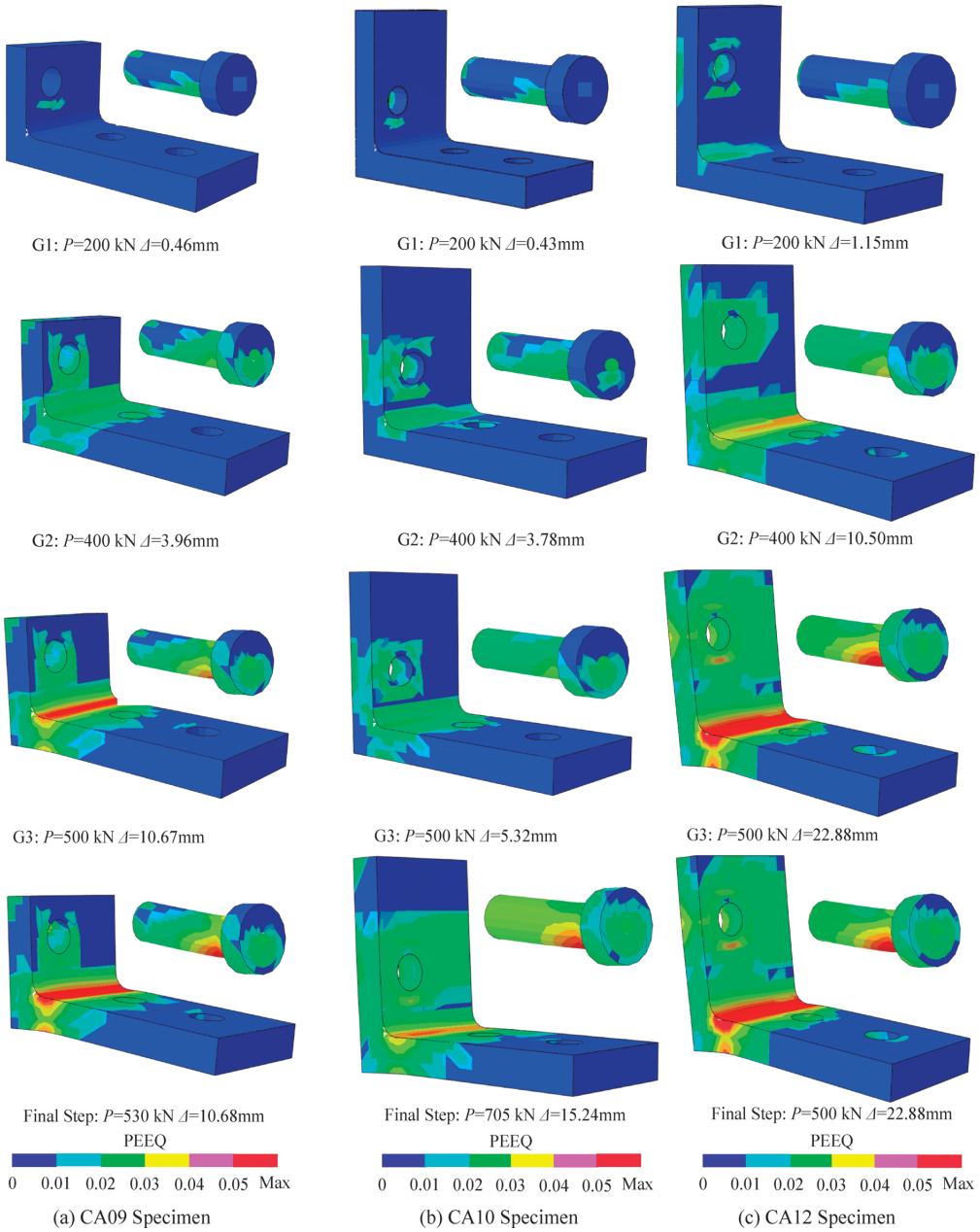

(a) CA09 Specimen (b) CA10 Specimen (c) CA12 Specimen

Fig. 12. Comparisons of the plastic deformation in the clip-angles from FE models.

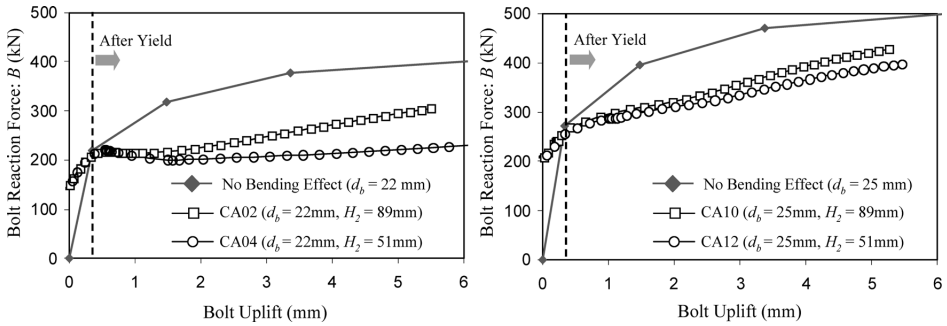

Fig. 10. Reaction force and deformation of tension bolts.

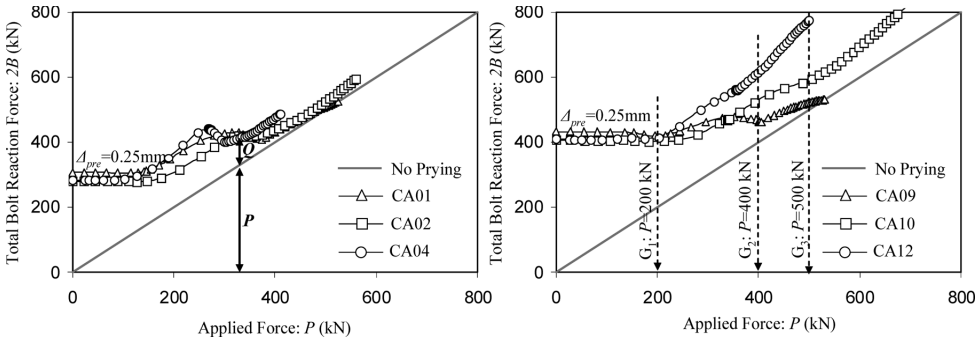

Fig. 11. Prying response of tension bolts.

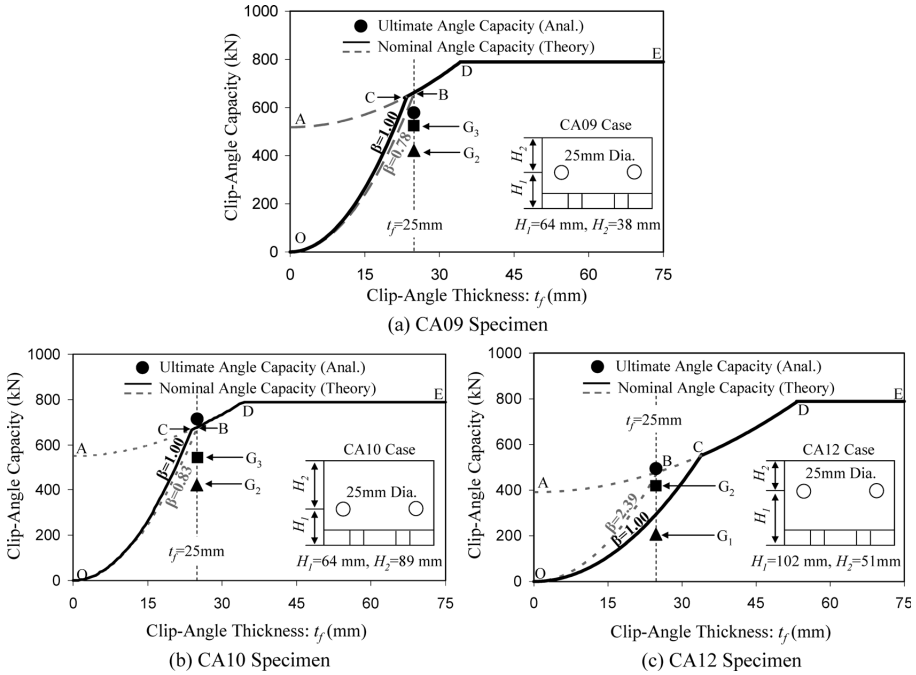

Fig. 13. General determination for the clip-angle capacity.

for such a failure by rupture or fracture, while others indicate design limit states based on yielding of the members. In this section, the ultimate capacity of heavy clip-angles will be investigated with existing experimental test results and FE analysis results.

The determination of the ultimate capacity of a clip-angle is illustrated in **Fig. 13**. Three specimens having the same geometric parameters, except for H_1 and H_2, were selected in order to examine the ultimate capacity and the failure mode with respect to the amount of bolt prying action. The detail description for the general solution to determine the clip-angle capacity was already described in the prying model (Sec. 2). Thus, based on the observation of FE models after analyses, we mainly investigate herein whether the solution space can reflect on the failure mode or not. To achieve this purpose, the axial forces at each loading step graphically described in Figs. 11 and 12 are plotted on the theoretical solution space (see Fig. 13).

For CA09 and CA10 specimen, the point B corresponding to the ultimate capacity of the clip-angle component

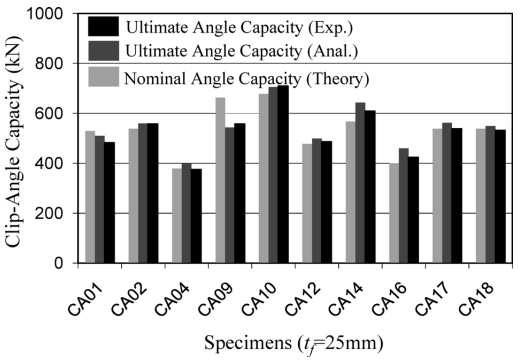

Fig. 14. Clip-angle capacity and slip resistance of all specimens.

with t_f=25 mm lies on the line segment CD. Since the line segment OB is located on the region where the prying parameter (β) is within the range of 0 to 1, the plastic flange mechanism does not occur during the loading step (see G_2 and G_3 plotted in Figs. 13(a) and 13(b)). Therefore, both specimens are expected only to fail by the bolt fracture simultaneously combined with flange yielding under the ultimate state. It agrees with the observation of the plastic deformation shown in Figs. 12(a) and 12(b). The ultimate clip-angle capacity of CA10 specimen is approximately 3% larger than the predicted clip-angle capacity on the solution space. However, the predicted clip-angle capacity of CA09 specimen is unconservative by the value of approximately 16%.

In case of CA12 specimen, the axial force at the first loading step (*i.e.* G_1=200 kN) is anchored below the line segment OC (see Fig. 13(b)). It coincides with the fact that the clip-angle under the first loading step (*i.e.* G_1=200 kN) does not show any failure modes as shown in Fig. 12(c). The axial force at the second loading step (*i.e.* G_2=400 kN) is located in the domain OBCO. It also agrees with the occurrence of the plastic mechanism on the clip-angle leg as shown in this figure. Finally, the ultimate clip-angle capacity of CA12 specimen corresponding to 500 kN slightly exceeds the line segment ABC.

In an effort to avoid catastrophic collapse, the ultimate capacity of the clip-angle based on the tension bolt fractures should lie on or just above the predicted clip-angle capacity which is represented by the point B on the theoretical solution space. This predicted capacity indicates the requirement of strength for the connection design. For all specimens provided, the ultimate clip-angle capacities obtained by FE and experimental tests are compared with their predicted clip-angle capacities, as shown in **Fig. 14**. Except for CA01 and CA09 specimen, the ultimate strength of clip-angles exceeds the predicted clip-angle capacity. It indicates that the strength prediction of clip-angle components presented in this study is restricted to the clip-angle component with the moderate length of the H_2 parameter ($H_2 \geq 51$ mm). Overall, the line segment ABD results in a conservative capacity prediction.

8. Concluding Summary

A 3D FE solid model for thick angle components and connections utilizing both contact interactions and non-linear material properties provided good results when compared to experimental results. This FE model successfully predicted contact interaction, prying force mechanisms, and slip deformation identical. In addition:

(1) The overall deformation of the clip-angle was captured well by the FE model, which correctly predicted the sequence of sliding, bearing contact, and development of a prying mechanism.

(2) Large displacements were reached due to bending of the tension bolts during the prying. Some models (CA04, CA12) showed more visible prying action, as evidenced by deteriorating axial capacity and distinct yield lines at the tension bolts.

(3) The coefficient of friction and the pretension of shear bolts result in a significant parameter to predict the slip load. Especially, the numerical value of a coefficient was determined from the level of slip resistance in FE tests. The value of 0.25 was accepted for the friction coefficient.

(4) The line segments, which are able to predict the design strength of clip-angle components on the solution space, were calculated by the prying model proposed by Kulak *et al.*[22] This prying model is based on available failure modes between clip-angle legs and tension bolts. The strength predictions based on this established prying model are adequate to estimate the ultimate capacity of heavy clip-angles except for the specimens having the relatively short length of upstanding clip-angle legs (*i.e.* CA09).

Acknowledgements

The experimental data generated as part of the SAC research project (SAC Subtask 7.03 performed at the Georgia Institute of Technology) under the sponsorship of the Federal Emergency Management Agency (FEMA) was used for this research. This research was supported by WCU (World Class University) program through the NRF (Ntional Research Foundation) of Korea funded by the Ministry of Education, Science and Technology (Grant No. R32-2008-000-20042-0). The first author would like to also thank the NRF of Koera for two years of financial support (Grant No. M06-2003-000-10009-0) as a government graduate scholarship student.

REFERENCES

1) J. Liu and A. Astaneh-Asl: *J. Struct. Eng., ASCE*, **126** (2000), No. 1, 32.
2) T. Kim and B. Han: *ISIJ Int.*, **47** (2007), No. 6, 920.
3) J. Yang and S. Jeon: *IJOSS, KSSC*, **9** (2009), No. 3, 195.
4) R. T. Leon: *Eng. Struct.*, **20** (1998), 364.
5) J. C. Awkar and E. M. Lui: *Eng. Struct.*, **21** (1999), No. 5, 425.
6) J. A. Swanson and R. T. Leon: *J. Struct. Eng., ASCE*, **126** (2000), No. 1, 50.
7) J. A. Swanson and R. T. Leon: *J. Struct. Eng., ASCE*, **127** (2001), No. 5, 498.
8) G. Shi, Y. Shi and Y. Wang: *Eng. Struct.*, **29** (2007), No. 5, 703.
9) A. Azizinamini, J. H. Bradburn and J. B. Radziminiski: *J. Constr. Steel Res.*, **8** (1987), 71.
10) A. Azizinamini and J. B. Radziminiski: *J. Struct. Eng., ASCE*, **115** (1989), No. 12, 2979.
11) F. H. Wu and W. F. Chen: *Eng. Struct.*, **12** (1990), No. 2, 88.
12) S. Lee and T. Moon: *Eng. Structt.*, **24** (2002), No. 2, 227.
13) L. Calado: *Eng. Struct.*, **25** (2003), No. 9, 1189.
14) A. Pirmoz , A. S. Khoei, E. Mohammadrezapour and A.S. Daryan: *J. Constr. Steel Res.*, **65** (2009), 973.
15) J. A. Swanson: Ph.D. Dissertation, Georgia Institute of Technology, (1999).

16) C. S. Schrauben: Master's Thesis, Georgia Institute of Technology, (1999).
17) J. A. Swanson, D. K. Kokan and R. T. Leon: *J. Constr. Steel Res.*, **58** (2002), 1015.
18) J. Hu and R. T. Leon: Proc. of 3rd Int. Symp. on Steel Structure, ISSS, Korean, (2005).
19) J. Hu: Ph.D. Dissertation, Georgia Institute of Technology, (2008).
20) A. M. Citipitioglu, R. M. Haj-Ali and D. W. White: *J. Constr. Steel Res.*, **58** (2002), 995.
21) American Institute of Steel Construction (AISC): Manual of Steel Construction: Load and Resistance Factor Design (LRFD), 3rd ed., Chicago, IL, (2001).
22) G. L. Kulak, J. W. Fisher and J. H. A. Struik: Guide to Design Criteria for Bolted and Riveted Joint, 2nd ed., Johns Wiley & Sons, (1987).
23) W. A. Thornton: *J. Eng., AISC*, **22** (1985), No. 2.
24) Habbit, Karlsson and Sorenson Inc.: Standard User's Manual, ABAQUS, (2006).